Heat capacity in a model polydisperse ferrofluid with narrow particle size distribution

Tamás Kristóf and János Liszi
Department of Physical Chemistry, University of Veszprém, H-8201 Veszprém, P.O. Box 158, Hungary

István Szalai
Department of Physics, University of Veszprém, H-8201 Veszprém, P.O. Box 158, Hungary
(Received 23 November 2004; published 23 March 2005)

The influence of polydispersity on the phase equilibrium properties and the heat capacity of a dipolar system with additional short-range (repulsive+attractive) interactions (modeled by a shifted Lennard-Jones pair potential) is studied by means of a Monte Carlo scheme. The particle distribution of the investigated system is realized in the semigrand ensemble by tuning appropriately the underlying particle distribution density. The phase coexistence and heat capacity data are calculated with and without an applied magnetic field, and the obtained results are compared with the data determined in a monodisperse equivalent of the system.

DOI: 10.1103/PhysRevE.71.031109 PACS number(s): 05.20.Jj, 64.70.Fx, 75.50.Mm, 82.20.Wt

I. INTRODUCTION

Ferrofluids or magnetic fluids are stable colloidal dispersions of nanometric magnetic particles coated with ionic groups or polymer surfactants in liquid carriers [1]. Since the constituent nanoparticles can interact easily with external magnetic fields, and the ferrofluid properties can be effectively controlled by these fields, ferrofluids have a wide range of potential applications. These nearly spherical nanoparticles possess permanent magnetic dipole moments, which are proportional to their volumes. Therefore, in addition to the usual spherically symmetric interactions, van der Waals attractions and electrostatic or steric repulsions, long-range dipolar particle interactions play a key role in the thermodynamic properties of ferrofluids. When studying theoretically ferrofluids thermodynamics, especially the equilibrium magnetization and phase transitions, these fluids are generally treated as dipolar fluids, where only the colloidal particles are explicitly taken into account [2–11].

An inherent feature of real ferrofluids is that the nanoparticles differ in size and magnetic moment. This polydispersity affects the equation of state of the system and may have important consequence for the phase behavior, in particular for the fluid-fluid coexistence [12,13]. This property also affects the equilibrium magnetization for dense as well as for diluted liquids. Recently, the influence of realistic polydispersity on the equilibrium magnetization properties of model ferrofluids was investigated by simulation, and it was found that the magnetization is generally higher in the polydisperse system than in its monodisperse equivalent [14]. Such simulation studies generally operate with a discretization of the particle distribution, reducing the number of components to a small value. A more sophisticated approach involves employing the semigrand ensemble: this technique allows simulations with quasicontinuous particle distributions and thus finite-size effects become insignificant in such calculations. However, this technique was originally restricted to systems with variable polydispersity, i.e., to systems where the form of the particle distribution also depends on the thermodynamic conditions, because the particle distribution is controlled by the imposed chemical potential difference distribution [15–17]. For systems with fixed polydispersity, such as ferrofluids (where the particle distribution is set when creating the system), methods has been recently developed within a grand canonical framework [18,19] to overcome the difficulty associated with the need to determine the form of the underlying (sampling) distribution for which the ensemble averaged particle distribution matches the target particle distribution.

In this paper, our main concern is the influence of fixed polydispersity on the heat capacity of a dipolar system exhibiting a fluid-fluid phase transition. Phase coexistence is determined in a dipolar system with reduced polydispersity, and isochoric heat capacities are calculated in the dense and in the diluted phases. Using a simple scheme a quasicontinuous particle distribution is realized in the simulations. The obtained results are compared with the data determined in a monodisperse equivalent of the system. In this work, a relatively small degree of polydispersity is adopted with the intention of obtaining phase diagrams as similar as possible for the polydisperse and monodisperse systems, in order that the single phases of the polydisperse and monodisperse systems be in nearly "corresponding states" at the same densities.

II. METHOD

A. Model

The system consists of spherical particles of diameter σ_i, which have permanent point dipole (magnetic) moments m_i. The short-range repulsive interaction and the van der Waals attraction between particles i and j are modeled by a shifted Lennard-Jones pair potential:

$$\varphi_{ij}^{r} = 4\varepsilon\left[\left(\frac{\sigma_{ij}}{r_{ij}-\zeta}\right)^{12} - \left(\frac{\sigma_{ij}}{r_{ij}-\zeta}\right)^{6}\right], \tag{1}$$

where ε is the energy parameter, r_{ij} is the interparticle distance, $\sigma_{ij}=(\sigma_i+\sigma_j)/2$, and ζ is an additional size parameter. Shifting in the distance scale allows a crude approximation to take into account the fact that, due to the presence of stabilizing nonmagnetic layers, the particle size in ferrofluids exceeds the magnetic core diameter σ_i.

The dipole-dipole potential between particles i and j is given by

$$\varphi_{ij}^{d} = \frac{1}{4\pi\mu_0}\left[\frac{\mathbf{m}_i \cdot \mathbf{m}_j}{r_{ij}^3} - 3\frac{(\mathbf{m}_i \cdot \mathbf{r}_{ij})(\mathbf{m}_j \cdot \mathbf{r}_{ij})}{r_{ij}^5}\right], \tag{2}$$

where μ_0 is the permeability of vacuum, and the interaction of dipole moments with an external magnetic field $\mathbf{H}$ can be written as

$$\varphi_i^{\text{ext}} = -\mathbf{m}_i \cdot \mathbf{H}. \tag{3}$$

In our previous paper [13], we obtained a much narrower fluid-fluid coexistence envelope for this shifted Stockmayer model than for the original Stockmayer model [6]. The introduction of the additional size parameter ζ yields smaller liquid and greater vapor densities, as well as a lower critical temperature.

The particle polydispersity is described by the gamma distribution [20]

$$f(x) = \frac{\zeta}{x_0}\left(\frac{x}{x_0}\right)^a \quad \frac{\exp(-x/x_0)}{\Gamma(a+1)}, \tag{4}$$

where x is the magnetic core diameter of particles, x_0 and a are the parameters of the distribution, Γ denotes the gamma function, and ζ is taken as the unit length [to render $f(x)$ dimensionless]. For spherical particles, $\sigma = x$, and the magnetic moment reads

$$m = \mu_0 M_d \frac{\pi}{6} x^3, \tag{5}$$

where M_d represents the bulk magnetization of the ferromagnetic component.

B. Monte Carlo algorithm

One- and two-phase constant volume and temperature Monte Carlo calculations have been performed using the above model. In addition to the usual translational and orientational moves of the particles (one-phase canonical simulations) as well as volume and particle transfer moves (two-phase Gibbs ensemble [21] simulations), resizing moves were also invoked to realize a size distribution of particles in the system.

The procedure we constructed to produce appropriate distribution functions for the trial moves responsible for generating the possible configurations of particle sizes is the following.

We started from a semigrand ensemble scheme that operates with resizing moves by sampling from a fixed underlying particle distribution density $f_u(x)$ (this is equivalent to sampling by means of a chemical potential difference distribution) [16,17]. In our case, however, $f_u(x)$ is dynamically updated during the simulation in such a way as to minimize the deviation of the instantaneous particle distribution density $f_c(x)$ from the target distribution density $f(x)$. As an initial guess, either $f_u(x) = f(x)$ is set, or $f_u(x)$ is taken from the output of a previous run. The distributions are stored in the form of a histogram with a prescribed number of subintervals ("bins"). At regular simulation intervals, the histogram approximation of $f_u(x)$ is adjusted bin by bin: for each entry x_i, its value is increased by 5% if $f_c(x_i) < f(x_i)$, and decreased by 5% if $f(x_i) < f_c(x_i)$, and its value is kept unchanged if $f_c(x)$ agrees with $f(x)$ within 0.1%. Here, $f_c(x)$ is taken from a limited number of configurations immediately preceding the adjustment step (this procedure is similar to that followed frequently in conventional Monte Carlo simulations for tuning the maximum allowed displacement of particles to get a desired acceptance ratio [22]). Finally, after considering all of the entries in the adjustment step, the new approximation of the underlying particle distribution density is renormalized appropriately. The imposed small value for the adjustment parameter (5%) ensures that a change at any entry only very slightly affects $f_c(x)$ at other entries in the subsequent simulation interval.

Tuning $f_u(x)$ in this manner violates detailed balance. Nevertheless, when employing a relatively long equilibration period in the simulations, the fluctuations in the histogram approximation of $f_u(x)$ become small and the production run is completed with an *effectively* unchanging $f_u(x)$. Alternatively we can take the "ensemble averaged" underlying particle distribution density as the input of a normal semigrand ensemble simulation. This can be done also in the case of the two-phase simulations.

C. Computational details

In the calculations $N = 500$ (one-phase simulations) and 1000 (two-phase simulations) particles were employed. The production period of the simulations varied between 400×10^6 and 600×10^6 trial moves. The frequency of attempting resizing moves was equal to that of the translational and orientational moves and, likewise, the acceptance criterion of the resizing moves was the same as that used for the translational and orientational moves [15].

Standard long-range corrections were applied for the Lennard-Jones-type interaction assuming that the pair correlation functions are unity beyond the cutoff radius [22]. The long-range dipolar interactions were treated using the Ewald summation with conducting boundary condition [23]: in this case the applied external field is identical to the internal field acting on particles throughout the simulation box.

The results for the dipolar (magnetic) fluids are presented in reduced units, where the mean magnetic core diameter $\bar{x}$ is used for σ: $T^* = kT/\varepsilon$ is the reduced temperature with k being the Boltzmann constant, $\rho^* = N\sigma^3/V$ is the reduced density, $p^* = p\sigma^3/\varepsilon$ is the reduced pressure, $u^* = U/(\varepsilon N)$ is the reduced potential energy, and $c_V^* = C_V/(kN) = (\partial u^*/\partial T^*)_V$ is the dimensionless form of the configurational isochoric heat capacity. Furthermore, the dimensionless forms of the magnetization and the external magnetic field are $M^* = M/\sqrt{4\pi\varepsilon/(\mu_0\sigma^3)}$ and $H^* = H\sqrt{4\pi\mu_0\sigma^3/\varepsilon}$, respectively, and $m^{*2} = m^2/(4\pi\mu_0\varepsilon\sigma^3)$ is the reduced squared magnetic moment. For the magnetic coupling, $\lambda = m^{*2}/T^* = 1$ was adopted at $T^* = 1$. This choice implies that the average reduced magnetic moment was *unity* in all calculations.

In the simulations the equilibrium magnetization can be obtained from the expression

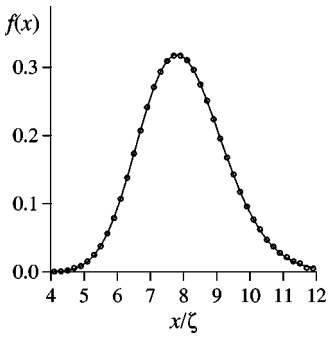

FIG. 1. The applied particle distribution density for the polydisperse system. Data points show the measured distribution in one-phase simulation at $T^*=1.05$ and $\rho^*=0.44$, and the continuous line indicates the target distribution.

$$\mathbf{M}=\frac{1}{\mu_0}\left\langle \sum_{i=1}^{N}\frac{\mathbf{m}_i}{V}\right\rangle, \tag{6}$$

where the brackets denote the ensemble average. The configurational isochoric heat capacity was determined from one-phase simulations in two ways: for the monodisperse system, directly from the fluctuations of the potential energy ($kT^2C_V=\langle U^2\rangle-\langle U\rangle^2$) and, for the polydisperse system, through temperature differentiation of a fit to the average potential energy data obtained at four distinct temperatures close to the target temperature (at a given density). Utilizing the second method, several results for the monodisperse system were cross-checked.

To achieve a relatively narrow distribution, $x_0/\zeta=0.2$ and $a=39$ were taken, and the unit length was set to 1 nm [13]. This gamma distribution reproduces the peak height and the peak width at half maximum of a normal (Gaussian) distribution with $\overline{x}=7.8$ nm and $s/\overline{x}=0.16$ (where s is the standard deviation), but it has a slower decay in the range of large diameters. We truncated the particle distribution at 4 and 12 nm, where $f(x)$ is already well below 0.005. Nonetheless, this truncation leads to a decrease of the original mean core diameter, $\overline{x}=x_0(a+1)=8$ nm, by 0.4%. The histogram discretization parameter (the width of the particle size subintervals or bins) was set to 0.2 nm.

According to our experience, it was unnecessary to perform normal semigrand ensemble simulations with "ensemble averaged" underlying particle distribution density as we checked that, in the present case, the simulations with dynamically adjusted $f_u(x)$ yield the same results both for the structure and thermodynamics. The sole difficulty with implementing the original procedure at higher densities was that the measured distribution failed to fully match the values in the "wings" of $f(x)$. To cure this problem, in those ranges of diameters for which $f(x)$ is very small the adjustment parameter was set proportional to the relative deviation of $f_c(x)$ from $f(x)$ allowing this parameter to vary up to a maximum slightly increased from 5%. Figure 1 illustrates the good agreement between the target particle distribution and that obtained in the simulations.

D. Exploring the phase space

The phase coexistence was studied at fixed number densities of the starting (parent) phase. This corresponds to the experimental procedure that involves adding a prescribed quantity of particles with a given degree of polydispersity to a vessel of fixed volume and observing possible phase separations. In this manner, two-phase separations occur with fixed global particle distribution density but, naturally, the distribution densities of the coexisting phases differ from that of the parent phase. This study was restricted only to the fluid phases; it is known that magnetic fluids exhibit vapor-liquid-like phase separation, i.e., coexistence of a dense liquid phase with a diluted liquid phase.

Theoretically (i.e., disregarding finite-size effects in the simulations), phase coexistence results can be obtained up to the temperature for which the density of either phase becomes equal to the density of the parent phase. At this end point of phase equilibrium, called the cloud point, the amount of the other coexisting phase is negligible. The coexistence density curves meet at the critical temperature T_c only if the density of the parent phase is equal to the critical density ρ_c. Accordingly, the critical point for this system can be determined solely by an iterative procedure. First, a pseudocritical density is estimated for a selected density of the parent phase $\rho_0^{(0)}$ using the Gibbs ensemble simulation results at various temperatures up to the end point. Assuming a Wegner expansion [24] and neglecting the contribution from the gap exponent [25], the dense (L) and the diluted (V) phase densities can be fitted to the expression

$$\rho_{L,V}=\rho_c\pm B(1-T/T_c)^{\beta}+C(1-T/T_c), \tag{7}$$

where B and C are parameters and β is the critical exponent which is set to its exact nonclassical value 0.325. The coexistence curves are then determined for $\rho_0^{(1)}=\rho_c^{(0)}$, and the procedure is repeated until $\rho_c^{(n)}$ agrees with $\rho_0^{(n)}$ within the uncertainty of the calculation. It should be noted that the obtained critical points are approximate in the sense that they are determined without performing a finite-size scaling study.

Having located the critical point, a rough estimation of the cloud curves in the low- and high-density sides of the critical coexistence envelope was performed. Since outside the cloud curve only single phases are stable, the density of the parent phase was gradually increased at constant temperature until the termination of phase coexistence was observed (the low-density phase disappeared). The density of the cloud point in the high-density side was determined by extrapolation taking into account some finite size effects. Gradually decreasing the density of the parent phase, the cloud point in the low-density side was estimated in a similar way.

III. RESULTS AND DISCUSSION

We compare the fluid-fluid coexistence results of our polydisperse system with those of a monodisperse system. The monodiperse fluid is characterized by uniform σ and m,

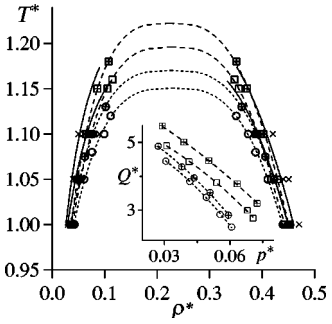

FIG. 2. Coexistence densities for the monodisperse fluid [13] (circles and dotted lines) and for the polydisperse fluid for which the density of the parent phase is identical to the critical density (squares and dashed lines). In both cases, $\overline{m}^*=1$. Open symbols and symbols filled with (+) represent results obtained at $H^*=0$ and 1, respectively. The continuous lines are the estimated cloud curves: the two inner lines correspond to the results obtained in the absence of the external field. The inset contains the heat of phase change as a function of the coexistence pressure. State points where heat capacities were calculated from one-phase simulations are marked with crosses.

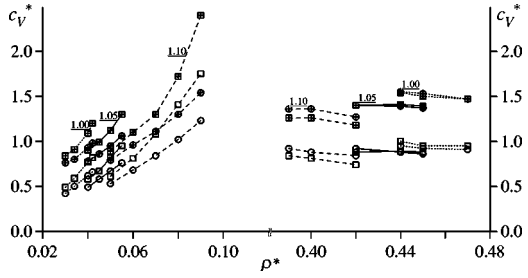

FIG. 3. Configurational heat capacities for the monodisperse (circles) and for the polydisperse fluid (squares). Open symbols and symbols filled with (+) represent results obtained at $H^*=0$ and 1, respectively. Points corresponding to $T^*=1.00$, 1.05, and 1.10 are connected by dotted, continuous, and dashed lines, respectively.

with the additional specification that $m^*=1$. Due to the fact that $\overline{m}\propto\overline{x^3}$ and $\overline{x^3}\neq\overline{x}^3$ for the polydisperse fluid, the monodisperse fluid can be considered to have either a different mean core diameter or different bulk magnetization (i.e., different ferromagnetic component) than those of the polydisperse fluid. As the choice of σ is arbitrary to some degree, the equivalent monodisperse system might be the one with the same volume fraction of the magnetic cores as the polydisperse system (at the same number density). This means that, instead of the mean core diameter, the mean cubed core diameter would be identical for the two systems. Nevertheless, this choice does not affect our numerical results presented in reduced units.

Figure 2 shows that the widths of the coexistence envelopes of the monodisperse system are more or less similar to those of the polydisperse system for which the density of the parent phase is identical to the critical density (the results for the monodisperse system are taken from our previous work [13]). In contrast with our earlier findings with a medium degree of polydispersity [13], the introduction of this reduced polydispersity slightly increases the density difference between the coexisting dense and diluted fluid phases. At the same time, the upward shift of the critical point is consistent with those obtained earlier [13,17]. Also, the broadening of the coexistence region of the polydisperse system with the field strength is expected [13]. The difference between the polydisperse system and its monodisperse counterpart looks more pronounced when considering the heat of phase change Q^* [$Q^*=\Delta u^*+p^*\Delta(1/\rho^*)$, where Δ refers to the change upon phase transition]. The distributions of particles in the coexisting polydisperse phases were found to be significantly different: the larger particles predominantly belong to the denser phase, and this causes an enlargement in the potential energy change associated with the phase transition. In our case, the distribution of the denser phase generally resembles the distribution of the parent phase; however, the closer we are to the critical temperature, the more the distribution of the denser phase differs from the parent distribution. This is the reason the estimated cloud curve, the distribution of which is by definition equal to the parent distribution, may cross the critical orthobaric density curve even in the high-density side.

It should be noted that while in the monodisperse phases practically no particle aggregation occurs, approximately 1%

TABLE I. Estimated critical properties for the monodisperse fluid [13] and for the polydisperse fluid (in both cases, $\overline{m}^*=1$). The numbers in parentheses represent the estimated uncertainties in the last digit.

	Monodisperse fluid		Polydisperse fluid	
H^*	T_c^*	ρ_c^*	T_c^*	ρ_c^*
0	1.151(5)	0.229(4)	1.196(5)	0.227(3)
1	1.170(5)	0.227(4)	1.223(5)	0.223(4)

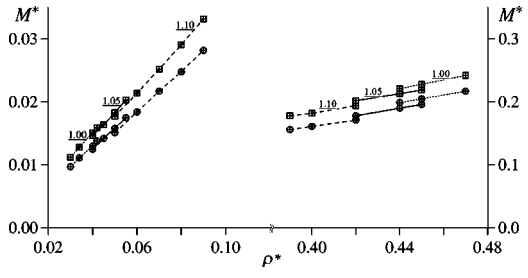

FIG. 4. Magnetizations for the monodisperse (circles) and for the polydisperse fluid (squares) at $H^*=1$. Points corresponding to $T^*=1.00$, 1.05, and 1.10 are connected by dotted, continuous, and dashed lines, respectively. Note that the two parts of the figure differ in the scale of the y axis.

of the particles of the high-density polydisperse phases can be found in clusters. These clusters were defined on the basis of the pair energies of the interacting particles [26]: two particles were considered to be bound if their potential energy is less than 75% of their contact energy in perfect coalignment. Although the clusters in the polydisperse phases are primarily flexible dimers and trimers, these might affect the fluid properties, especially the magnetic properties [27], to a greater extent. Nevertheless, the aggregation does not seem significant in our polydisperse system; moreover, as the amount of clusters reduces with decreasing ρ, the influence of clustering becomes completely negligible in the low-density side.

The estimated critical properties are shown in Table I. T_c^* is slightly greater in the polydisperse system than in the corresponding monodisperse one but ρ_c^* is roughly the same in both systems. According to the principle of corresponding states, a reduction with the critical properties would also make sense; for the polydisperse system, this will lower the reduced temperatures by approximately 4% as compared to those of the monodisperse system.

The locations of state points where the heat capacities were determined are indicated in Fig. 2 (the selected temperatures are $T^*=1.00$, 1.05, and 1.10). Here, in the inset we plotted the heat of phase change as a function of the coexistence pressure (instead of the temperature) to present our results also for the pressure. So this "composite" figure also reveals that, at the three selected temperatures, the coexistence pressure is roughly the same for the polydisperse system and for its monodisperse counterpart. For the heat capacity calculations the densities were chosen near the orthobaric density curves. Some points are *inside* the orthobaric density or the cloud curves, but on the basis of the increasing tendency of the pressure with the increasing density obtained from one-phase simulations at constant temperature, it was verified for both systems that all of these points are *outside* the spinodal curves (where the phase first becomes unstable to local density fluctuations).

The heat capacity results from one-phase simulations are presented in Fig. 3. It is seen that the configurational heat capacity reduces on passing from (the vicinity of) the two-phase region toward the interior of the single phase regions. The most striking feature of this figure is the marked contrast between the results obtained in the absence and in the presence of the external field. Under the influence of the external field, the relative increase in the temperature derivative of the potential energy may be as large as 60%. The absolute increase was found to be approximately equivalent to the lowering in the potential energy (in reduced units, according to the definitions given in Sec. II C); this is larger in the high-density side, which reflects the fact that the interaction of a system of dipoles with the external field is proportional to the density [14,27].

In the high-density side no clear distinction can be observed between the results for the polydisperse system and those of its monodisperse counterpart, except for $T^*=1.10$, where the monodisperse system possesses somewhat greater c_V^*. By contrast, in the low-density side the heat capacity for the polydisperse system consistently exceeds the corresponding value for the monodisperse system. There are two densities in the low-density side ($\rho^*=0.04$ and 0.05) where the results obtained at different temperatures can be compared. Here, we find that the heat capacity of the monodisperse system at $T^*=1.00$ is approximately equal to that of the polydisperse system at $T^*=1.05$, and the same holds for the results at $T^*=1.05$ and 1.10, which means that the corresponding c_V^* data are approximately equal for the two systems at the same T^*/T_c^* and ρ^*/ρ_c^* (recall that T_c^* is about 4% higher in the polydisperse system). This rule does not work for the high-density side, where such a comparison reveals that, at the same T^*/T_c^* and ρ^*/ρ_c^*, the monodisperse system possesses greater c_V^*. The fact that no polydispersity-induced increase in this caloric property was found here is somewhat surprising, since the potential energy is consistently 5–10 % lower in the polydisperse system (these results are not shown here) and the two systems are quite dissimilar also in magnetic character. The latter is illustrated in Fig. 4, where the calculated equilibrium magnetization is shown in the presence of the external magnetic field (M^* is practically zero in the absence of the external field in all cases). As can be seen, M^* is significantly greater in the polydisperse system than in the monodisperse one, especially in the high-density side, which suggests that the contribution of the particles with magnetic moments larger than the mean magnetic moment to the system's properties is crucial.

In summary, we considered the effect of polydispersity on the phase behavior and the isochoric heat capacity data of a model ferrofluid with reduced polydispersity. The obtained fluid-fluid equilibrium curves reflect the dissimilarity in composition and thus in structure between the polydisperse system and its monodisperse counterpart. At the same time, the heat capacity was found to be rather insensitive to the composition variations in the denser phase. Nevertheless, the calculations provide evidence of the large influence of the external magnetic field on the temperature derivative of the potential energy of our dipolar systems.

The proposed technique has proved to be a promising tool for simulating systems with fixed polydispersity. It should be stressed that its implementation is simple and straightforward, and requires only a minor modification of the original semigrand ensemble procedure. In comparison with the more sophisticated grand canonical approach [19,28], where a self-consistent iterative determination of the chemical potential distribution (conjugate to the composition distribution) is performed, the new technique works with fixed overall number density, which makes it easier to handle the system in one-phase simulations. Notwithstanding these advantages, the work presented here was computationally demanding, because rather long calculations are needed to sample appropriately the low-probability particle size regions.

ACKNOWLEDGMENTS

The authors give due thanks to the National Information Infrastructure Development Office (NIIF) for providing computing time on their supercomputer. Financial support from the Hungarian Scientific Research Fund (Grant No. OTKA-TO38239) is acknowledged.

[1] R. E. Rosensweig, *Ferrohydrodynamics* (Cambridge University Press, Cambridge, U.K., 1985).
[2] M. E. van Leeuwen and B. Smit, Phys. Rev. Lett. **71**, 3991 (1993).
[3] B. Groh and S. Dietrich, Phys. Rev. Lett. **72**, 2422 (1994).
[4] B. Groh and S. Dietrich, Phys. Rev. E **53**, 2509 (1996).
[5] B. Groh and S. Dietrich, Phys. Rev. E **54**, 1687 (1996).
[6] M. J. Stevens and G. S. Grest, Phys. Rev. E **51**, 5976 (1995).
[7] R. van Roij, Phys. Rev. Lett. **76**, 3348 (1996).
[8] M. A. Osipov, P. I. C. Teixeira, and M. M. Telo da Gama, Phys. Rev. E **54**, 2597 (1996).
[9] J. M. Tavares, M. M. Telo da Gama, and M. A. Osipov, Phys. Rev. E **56**, R6252 (1997).
[10] P. I. C. Teixeira, J. M. Tavares, and M. M. Telo da Gama, J. Phys.: Condens. Matter **12**, R411 (2000).
[11] B. Huke and M. Lücke, Rep. Prog. Phys. **67**, 1734 (2004).
[12] A. O. Ivanov, J. Magn. Magn. Mater. **201**, 234 (1999).
[13] T. Kristóf, J. Liszi, and I. Szalai, Phys. Rev. E **69**, 062106 (2004).
[14] T. Kristóf and I. Szalai, Phys. Rev. E **68**, 041109 (2003).
[15] D. A. Kofke and E. D. Glandt, J. Chem. Phys. **87**, 4881 (1987).
[16] M. R. Stapleton, D. J. Tildesley, and N. Quirke, J. Chem. Phys. **92**, 4456 (1990).
[17] T. Kristóf and J. Liszi, Mol. Phys. **99**, 167 (2001).
[18] F. Escobedo, J. Chem. Phys. **115**, 5642 (2001).
[19] N. B. Wilding and P. Sollich, J. Chem. Phys. **116**, 7116 (2002).
[20] M. I. Shliomis, A. F. Pshenichnikov, K. I. Morozov, and I. Yu. Shurubor, J. Magn. Magn. Mater. **85**, 40 (1990).
[21] A. Z. Panagiotopoulos, Mol. Phys. **61**, 813 (1987).
[22] M. P. Allen and D. J. Tildesley, *Computer Simulation of Liquids* (Clarendon Press, Oxford, 1987).
[23] S. W. de Leeuw, J. W. Perram, and E. R. Smith, Proc. R. Soc. London, Ser. A **373**, 27 (1980).
[24] F. J. Wegner, Phys. Rev. B **5**, 4529 (1972).
[25] L. Vega, E. de Miguel, L. F. Rull, G. Jackson, and I. A. McLure, J. Chem. Phys. **96**, 2296 (1992).
[26] D. Levesque and J. J. Weis, Phys. Rev. E **49**, 5131 (1994).
[27] Z. Wang, C. Holm, and H. W. Müller, Phys. Rev. E **66**, 021405 (2002).
[28] N. B. Wilding, J. Chem. Phys. **119**, 12163 (2003).